Journal of Hazardous Materials 198 (2011) 151–158

Contents lists available at SciVerse ScienceDirect

Journal of Hazardous Materials

journal homepage: www.elsevier.com/locate/jhazmat

The interstitial location of selenium and arsenic in rocks associated with coal mining using ultrasound extractions and principal component analysis (PCA)

I. Pumure[a,*], J.J. Renton[b], R.B. Smart[c]

[a] College of Science and Technology, School of Environmental, Physical and Applied Sciences, University of Central Missouri, PO Box 800, Warrensburg, MO 64093, USA
[b] Department of Geography and Geology, West Virginia University, PO Box 6300, Morgantown, WV 26506, USA
[c] C. Eugene Bennett Department of Chemistry, West Virginia University, PO Box 6045, Morgantown, WV 26506, USA

ARTICLE INFO

Article history:
Received 29 March 2011
Received in revised form 6 October 2011
Accepted 6 October 2011
Available online 15 October 2011

Keywords:
Ultrasound extraction
Mountaintop removal/valley fill mining
Principal component analysis
Arsenic
Selenium

ABSTRACT

The release of selenium and arsenic from coal mine wastes into main waterways is an environmental cause for concern in the mining industry due to a myriad of subsequent ecotoxicological problems associated with the two metalloids. In a 2002 USEPA study undertaken in a mountaintop removal/valley fill (MTR/VF) mining area in southern West Virginia, measured Se concentrations were higher than the stipulated 5 ng/mL in 66 out of the 213 water samples collected. We studied the chemical composition of forty seven randomly selected pulverized core rock samples collected from depths of 25 ft to 881 ft from MTR/VF sites to determine the amounts of bioaccessible (ultrasound leachable) As and Se concentrations and their tentative locations within the rock matrix. The application of principal component analysis (PCA) to the chemical data, suggested that ultrasound leachable selenium concentrations were associated with 14 Å *d*-spacing phyllosilicate clays (chlorite, montmorillonite and vermiculite all 2:1 layered clays) whilst ultrasound leachable arsenic concentrations were closely related to the concentration of illite, another 2:1 phyllosilicate clay. Negative correlations between leachable arsenic and selenium with kaolinite a 1:1 layered clay, were also observed. We used the observed negative correlations to rule out the presence of selenium or arsenic in 1:1 kaolinite. Hence mining waste from MTR/VF sites containing substantial amounts of illite and 14 Å *d*-spacing clays may require to be placed in priority landfills or valley fills.

1. Introduction

Mountaintop removal/valley fill (MTR/VF) is a coal mining process that involves the removal of mountaintops to expose beds of coal. After clearing trees, soil and waste rock are unearthed in search of coal beds. The rock waste material generated by the mining process is placed in adjacent valleys and streams creating valley fills. Consequently, selenium and arsenic have been reported to leach from the deposited mine wastes into nearby valley streams [1]. In a 2002 USEPA study undertaken in a MTR/VF mining area in southern West Virginia, measured selenium concentrations were higher than the stream standard, 5 ng/mL in 66 out of the 213 water samples collected [1].

Hardy and Cornu [2] suggested that the amounts of leachable trace elemental substances from silty soils was related to their location within the solid phase. Hence the sorption and mineralization of organic and inorganic compounds occurring before lithification could have played a critical role in the localization of these metalloids in the solid phase. Organic matter from phytoplankton and other sources have been shown to get sorbed, preserved and lithified on clay minerals and soils [3], a process commonly occurring during the formation of sedimentary rocks. Chlorite, a phyllosilicate, was found to have the highest adsorption partition coefficient compared to montmorillonite and kaolinite [3]. Such sorption interactions can introduce selenium and arsenic previously complexed by organic molecules into the rock lattice for intercalation, preservation and lithification [4]. The sites for preservation can depend on the affinities and the reactivities [3] of different clay constituents including the participation of biogeochemically active microorganisms [5]. Kaolinite (1:1 clay), illite (2:1 clay), montmorillonite (2:1 clay), vermiculite (2:1 clay), and chlorite (2:1 clay) were the most common phyllosilicate clays found in the sedimentary rocks studied. Collectively we referred the following 2:1 clays; montmorillonite, vermiculite, and chlorite as 14 Å *d*-spacing clays because of the common 14 Å basal repeat unit they share [6,7].

The Appalachian Mountains in southern West Virginia consist of a variety of siliciclastic sedimentary rocks and rhyolites [8]. The siliciclastic sedimentary rocks include sandstones, mudstones, claystones, and siltstones [8,9]. These sedimentary rocks

* Corresponding author. Tel.: +1 660 543 4143; fax: +1 660 543 4843.
E-mail address: pumure@ucmo.edu (I. Pumure).

0304-3894/$ – see front matter © 2011 Elsevier B.V. All rights reserved.
doi:10.1016/j.jhazmat.2011.10.032

are comprised of primary minerals that include plagioclases, biotite and garnet [10]. Those of Taconian age contain both sedimentary and metamorphic (polycrystalline quartz and chlorite schist) rock fragments, whereas Acadian and Alleghanian sandstones are dominated by metamorphic rock fragments (quartz–muscovite and quartz–chlorite schist, detrital mica, and polycrystalline quartz) [8]. Plagioclase dissolution is regarded to be the most important weathering reaction in silicate-dominated natural hydrologic systems especially with respect to Si and Al, which constitute neoformed clays [9]. The secondary clay minerals formed include vermiculite, illite, montmorillonite, chlorite, olivine, kaolinite, and gibbsite [10,11]. Major elements including alkali elements, SiO_2, and trace elements such as Th, Rb, Sr, Ba, Cs that are found in the clay mineral matrix are mobile during ocean-floor alteration and tectonic metamorphism at the solid-solution interface [12]. Such chemical reactions can also occur in surface waters resulting in the leaching of the major and minor elements from the phyllosilicate clays into the water column [13].

The interpretation of chemical data obtained from the analysis of natural rock matrix dissolution and disintegration is very complex, often leading to challenges faced in modeling the intricate natural rock associated chemical reactivities at the solid–solution interface. However principal component analysis (PCA) can be used effectively in analyzing the chemical data and to help unveil essential correlations between different samples and variables. PCA is an unsupervised non-parametric multivariate statistical technique [14,15] that is used to reduce data dimensionality by identifying similar patterns and variables through introducing new latent variables which are linear combinations of the observed or measured variables. This allows for data mining through pattern recognition and the streamlining of large data sets into smaller and easier to handle pieces of information. In large data sets, a multi-step hierarchical clustering using PCA can be used to deconvolute and streamline data into unrelated sub-components or sub-clusters that can be further decomposed by follow up application of PCA to identify closely related parameters [16]. A biplot [17] is often used to map out direct details on the relationships between samples and variables. In this work, PCA was used to analyze the chemical compositional data of core samples obtained from MTR/VF method of coal mining. The objective of the study is to provide the information leading to the location of Se and As in the clay minerals and then to provide avenues for prioritization and possible pre-treatment of different kinds of MTR/VF waste before and during disposal in valley fills or landfills.

2. Materials and methods

2.1. Sampling

Forty seven randomly selected pulverized core rock samples were collected from depths of 25 ft to 881 ft from MTR/VF sites. The core samples were collected by the West Virginia Geological and Economic Survey (WVGES) from Kayford Mountain which is situated at the intersection of Boone and Kanawha Counties, West Virginia, USA (81°21′31″W, 37°58′42″). Mineral analyses were performed using a Philips PW1200 X-ray diffraction unit, and elemental analyses were performed using a Philips 1420 X-ray spectrometer, courtesy of WVGES, results of which are shown in Tables 1 and 2. A total of 47 pulverized samples were randomly selected in this procedure. Samples are identified by a number that corresponds to a collection depth in feet, from the top of Kayford Mountain, West Virginia, USA.

The dominant clay minerals in the coal-associated rocks were found to be kaolinite and illite with lesser amounts of 14 Å *d*-spacing clays. At least 10 samples were randomly selected containing higher amounts of at least one of the following: % 14 Å *d*-spacing clays, % kaolinite, or % illite. These pulverized samples were also found to contain appreciable amounts of quartz, plagioclase, and K-Feldspar.

2.2. Experimental

The arsenic and selenium chemical species were extracted from the samples using the optimized ultrasound extraction procedure we previously developed [18]. 1.00 g of the pulverized rock sample was placed in a dried 38 mL water jacketed glass extraction cell followed by the addition of 10 mL of nanopure water at $24 \pm 1\,^{\circ}C$. The mixtures were treated with 200 W cm^{-2} of ultrasound power for a continuous 20 min to extract selenium. Another ultrasound extraction was performed for 25 min to optimally extract arsenic. The mixtures were then centrifuged at 3400 g for 20 min and the supernatant solutions were carefully decanted into clean 25 mL polyethylene vials. The individual extracts were filtered and analyzed for total selenium and arsenic using graphite furnace atomic absorption spectrophotometry (GFAAS) and Se(IV) by hydride generation AAS using a Varian Model 55B model [18]. Averaged results from the analysis of extracts using GFAAS are given in Table 2. The % RSD for all results obtained in the heterogeneous pulverized samples were below 15%. Mineral, XRD and XRF elemental analyses of all samples were performed, courtesy of WVGES.

3. Results and discussion

3.1. Primary PCA analysis

The application of principal components analysis using Minitab15.0 (Minitab Inc.) generated 18 orthogonal principal components and the first eight explained 94.6% of the total variation. All of the 18 principal components and their respective eigenvalues are shown in Table 3. The variable contribution to the first eight PCs and their eigenvalues are also given in Table 3.

The first three PCs (PC 1, PC 2, and PC 3) explained 74.0% of the total variance within all the measured parameters. PC 1 largely described the variation in trace elemental composition and PC 2 explained lithology properties and PC 3 was used to describe selenium variation.

The loading plot between PC 1 and PC 2 shown in Fig. 1 has four distinct groups A, B, C and D. Two clusters (A and B) are made up of two unique lithologies of sandstones that are based on the amounts of K-Feldspar ($KAlSi_3O_8$) and plagioclase feldspar (albite and anorthite). Anorthite ($CaAl_2Si_2O_8$) and albite ($NaAlSi_3O_8$) are Ca and Na plagioclases respectively [19]. Cluster A sandstones contain K-Feldspar and quartz while cluster B sandstones are associated with plagioclase (Na/Ca feldspar). Both the two clusters (A and B) originated from sandstones but were composed of different mineral compositions. In Fig. 2, the 2-dimensional sample score plot also show the two distinct sandstone clusters.

Samples 60, 61, 157, 337, 414, 432, and 479 belong to the K-Feldspar sandstone cluster while 448, 486, 505, 519, 639, 719, 771, and 791 belong to the plagioclase sandstone cluster. It appears that there was a transition from K-Feldspar to plagioclase feldspar as the rocks were exposed to the earth's surface. K-Feldspar sandstone samples were collected at depths closer to the surface whereas plagioclase sandstones were collected at depths of approximately 400 feet and lower. Generally, the sandstones were found to have low amounts of both arsenic and selenium as shown in Table 2; however, selenium is leached at faster rates from sandstones than claystones [20]. Therefore, sandstones contain more bioaccessible forms of selenium [20].

Table 1

Sample number	[a]Quartz (%)	[a]K-Feldspar (%)	[a]Plagioclase (%)	[a]Illite (%)	[a]Kaolinite (%)	[a]14 Å clays (%)	[b]Lithology
25	29.9	1.5	1.1	46.1	21.4	ND	Sandstone
60	81.0	3.2	ND*	6.80	9.10	ND	Sandstone
61	75.3	4.9	ND*	9.60	9.40	0.90	Sandstone
125	53.8	0.9	1.2	25.3	14.9	4.00	Claystone
157	70.6	3.9	0.3	10.4	11.8	2.50	Sandstone
181	44.9	1.2	1.5	37.8	7.50	7.10	Shale
211	60.9	3.9	0.7	16.9	13.6	3.90	Siltstone
241	54.0	1.9	0.9	25.7	10.9	6.70	Claystone
278	68.0	4.6	0.5	11.5	11.0	2.00	Shale
290	32.6	1.1	1.3	38.4	11.9	14.7	Shale
299	38.2	1.4	1.6	39.2	11.3	8.40	Shale
305	47.1	1.0	1.3	29.6	9.00	12.0	Siltstone
337	74.7	3.8	0.4	8.30	9.90	2.10	Sandstone
369	14.4	ND	0.9	60.2	12.3	8.10	Claystone
372	29.8	1.4	0.8	35.7	11.9	20.4	Shale
397	66.9	3.6	1.3	14.4	9.70	4.10	Sandstone
404	39.5	2.4	1.2	23.5	12.3	21.0	Shale
414	72.1	6.7	ND*	12.0	7.10	2.00	Sandstone
432	59.7	6.5	ND*	10.8	21.5	1.50	Sandstone
448	72.6	5.2	0.9	10.8	7.00	2.30	Sandstone
479	65.3	5.0	ND*	9.10	18.4	1.40	Sandstone
482	27.1	1.0	1.7	48.6	7.80	8.60	Shale
486	61.3	2.4	5.6	20.5	5.00	5.20	Sandstone
505	72.1	3.0	3.4	10.8	7.80	2.30	Sandstone
519	67.4	4.4	4.0	14.4	6.40	2.50	Sandstone
571	32.1	0.4	0.5	40.1	12.2	14.7	Claystone
572	27.7	0.8	1.2	34.6	14.5	21.0	Claystone
578	33.7	0.8	1.3	26.0	10.5	27.6	Shale
581	47.4	1.6	0.8	26.6	13.3	10.3	Shale
639	67.2	2.1	6.9	13.1	8.50	2.20	Sandstone
677	25.2	0.8	1.0	39.0	9.80	24.2	Shale
697	32.7	0.8	1.1	26.8	14.1	23.1	Shale
699	28.8	0.0	1.0	50.3	6.30	13.6	Claystone
700	22.6	0.5	0.9	46.6	7.50	21.9	Claystone
701	25.2	1.2	1.3	44.9	7.60	19.8	Claystone
719	61.7	3.6	8.1	15.4	6.50	4.40	Sandstone
764	34.2	1.0	2.8	40.6	7.60	13.1	Shale
769	27.0	1.0	1.2	47.0	9.90	12.5	Shale
771	50.6	0.8	6.2	22.3	12.4	6.90	Sandstone
776	30.0	1.0	1.3	44.5	9.50	13.7	Siltstone
778	31.9	1.2	1.1	43.6	8.90	13.2	Shale
791	56.0	2.9	0.7	21.7	11.1	7.60	Sandstone
818	60.4	2.6	8.8	16.4	7.90	4.00	Sandstone
831	28.5	1.2	0.8	37.7	8.90	23.0	Siltstone
834	31.1	1.1	3.3	44.3	6.70	13.5	Sandstone
857	49.5	1.3	7.7	22.3	12.9	6.30	Sandstone
881	28.8	0.5	0.9	41.0	13.9	14.8	Shale

[a]X-ray diffraction and [b]microscopy results, courtesy WVGES.
ND (not detected) < 0.01%.
* ND < 0.1%.

In Fig. 2, cluster C is comprised of the solitary kaolinite, cluster D consists of illite, 14 Å *d*-spacing clays, arsenic, selenite, and total selenium including trace elements Al, Ti, K, Fe and Mg. The information suggests that most trace elements (exception of Ca, P, Na, and partly K) are all associated with 14 Å *d*-spacing clays and illite. As shown in Figs. 1 and 2, claystones, shales and siltstones are all associated with 14 Å *d*-spacing clays and illite and only to a lesser extent with kaolinite. Samples 571, 572, 699, 700 and 701 are part of the 14 Å *d*-spacing clays that were found to have highest amounts of selenium as shown in Tables 1 and 2. The claystones, siltstones and shales generally had more selenium and arsenic compared to sandstones. A three-dimensional plot of PC 1, PC 2 and PC 3 can be used to further accentuate the differences between "shales" and "sandstones" based rock samples. Such a three dimensional score plot can be used as a training set in a computerized approach to allow for an instrumental based faster characterization and identification of clay soils or rock minerals through the analysis and differential weighting of the concentrations of major and minor constituents [21,22]. Attempts have already been made in the characterization of materials used in a smelting process [23]. This procedure can allow for a faster determination of treatment procedures for different kinds of mining waste.

3.2. Secondary PCA analysis

A secondary PCA was applied to identify the relationships between clay minerals with arsenic and selenium. The secondary PCA was performed on the most important variables: illite, 14 Å *d*-spacing clays, kaolinite, selenium, and arsenic.

Before the application of a secondary PCA, the individual 14 Å *d*-spacing clays, kaolinite, and illite concentrations were transformed into fractions that indicate their contribution to the total clay content (% illite + % kaolinite + % 14 Å *d*-spacing clays) in each sample.

The kaolinite fraction was mapped into % kaolinite/(total % clay content) in all samples. The % illite and % 14 Å *d*-spacing clays were also converted into their fractional contributions to the % total clay content. The loading plot of the secondary PCA is shown in Fig. 3.

PC 1a describes illite composition and PC 2a represents 14 Å *d*-spacing clays composition. As shown in Fig. 3 the 14 Å *d*-spacing clays fractional component clustered together with selenium

Table 2

Sample number	[a]K_2O (%)	[a]SiO_2 (%)	[a]Al_2O_3 (%)	[a]Fe_2O_3 (%)	[a]Na_2O (%)	[a]MgO (%)	[a]TiO_2 (%)	[a]CaO (%)	[a]P_2O_5 (%)	[b]Total Se (ng/g)	[b]Total As (ng/g)	[b]Se(IV) (ng/g)
25	5.75	63.87	26.68	0.83	0.22	1.02	1.54	0.22	0.08	10.30	6296	6.67
60	2.48	81.05	15.28	ND**	0.07	0.48	0.86	0.22	0.10	93.20	4200	ND**
61	2.47	79.51	15.70	0.87	0.07	0.43	0.79	0.23	0.12	17.20	2900	4.52
125	3.14	71.03	24.02	ND**	ND**	0.86	1.41	ND**	0.07	35.93	6017	ND**
157	2.59	79.66	17.50	ND**	ND**	0.66	0.37	ND**	0.10	3.900	2550	1.43
181	4.97	68.08	22.16	2.10	0.01	1.61	1.23	0.03	0.07	1.490	6909	ND**
211	3.59	73.34	20.03	1.28	ND**	1.06	0.88	0.04	0.12	34.33	2722	1.48
241	3.88	70.40	21.41	1.57	ND**	1.48	1.46	0.01	0.09	168.7	6676	64.0
278	4.72	64.12	21.90	6.02	0.01	1.82	1.29	0.14	0.13	26.00	2471	4.12
290	5.13	62.85	23.66	4.91	0.12	2.18	1.16	0.09	0.12	47.53	3887	1.90
299	5.44	65.29	25.14	1.44	0.07	1.33	1.29	ND**	0.07	63.07	7510	ND**
305	4.19	68.55	21.24	3.01	ND**	1.75	1.32	0.03	0.11	8.270	5329	7.72
337	2.69	79.48	16.37	0.63	ND**	0.78	0.14	0.26	0.10	44.20	2677	24.0
369	6.10	54.00	24.36	11.8	0.02	1.86	1.49	0.28	0.13	134.8	7305	21.5
372	4.84	64.71	22.00	4.75	ND**	2.36	1.44	0.05	0.09	63.33	5702	1.96
397	3.17	75.03	19.76	ND**	ND**	0.95	1.40	0.05	0.13	47.25	2262	1.60
404	4.90	64.84	22.50	4.55	ND**	1.99	1.28	0.04	0.11	58.07	3812	ND**
414	3.32	80.45	16.90	ND**	ND**	0.57	0.32	ND**	0.11	63.97	3506	ND**
432	3.16	76.11	19.00	0.44	ND**	0.62	0.44	0.52	0.10	25.60	1949	ND**
448	3.02	76.73	14.73	2.70	ND**	1.22	0.59	1.22	0.12	17.05	3178	ND**
479	2.67	79.12	17.13	0.72	ND**	0.56	0.03	0.16	0.10	23.20	1958	ND**
482	5.75	56.77	18.68	15.1	0.01	2.33	0.89	0.43	0.13	8.450	6457	5.30
486	3.49	73.69	18.22	1.03	0.94	1.25	1.33	0.13	0.17	5.700	3625	1.13
505	2.81	78.26	15.43	1.04	0.63	0.91	0.50	0.57	0.11	10.10	2895	0.95
519	3.03	76.27	16.20	1.67	0.72	1.06	0.82	0.36	0.13	5.200	4189	0.90
571	4.91	62.25	23.95	5.17	0.05	2.15	1.34	0.04	0.08	387.0	5800	ND**
572	4.36	63.96	22.55	5.56	0.05	2.28	1.35	0.04	0.10	236.6	4210	82.1
578	4.63	63.23	22.49	5.80	0.07	2.32	1.46	0.07	0.12	10.20	4236	6.40
581	3.28	65.07	19.88	8.53	ND**	1.73	1.23	0.21	0.16	5.900	2330	1.90
639	2.73	76.45	16.40	1.45	1.48	0.94	0.39	0.30	0.12	3.600	5267	0.90
677	5.12	62.13	22.13	6.57	0.10	2.42	1.43	ND**	0.09	15.70	5036	10.4
697	4.60	60.77	22.12	7.98	0.06	2.22	1.52	0.11	0.13	66.60	2790	9.85
699	5.98	62.24	24.31	4.14	0.22	1.99	1.37	ND**	0.06	121.9	6392	115
700	5.52	63.83	23.28	4.16	0.19	1.97	1.27	ND**	0.06	228.8	6572	92.8
701	5.73	62.37	23.41	5.02	0.25	2.12	1.24	ND**	0.07	239.0	5294	122
719	3.09	75.01	16.75	1.37	1.67	1.13	0.68	0.43	0.13	7.270	3385	6.23
764	4.57	62.83	20.77	7.07	0.56	2.28	1.35	0.26	0.15	12.90	6469	10.3
769	5.12	58.73	21.34	10.0	0.19	2.51	1.44	0.58	0.16	21.30	7320	18.4
771	2.75	68.08	18.93	5.46	1.13	1.76	1.15	0.73	0.18	10.30	4331	8.43
776	4.68	60.93	22.07	7.64	0.23	2.33	1.59	0.45	0.17	18.03	4296	15.3
778	4.97	61.54	21.15	8.19	0.10	2.34	1.35	0.33	0.15	19.43	6234	19.2
791	3.62	70.49	20.81	1.98	0.02	1.48	1.50	0.14	0.21	15.37	3560	9.13
818	3.01	72.90	17.93	2.36	1.77	1.20	0.61	0.33	0.13	13.93	3807	9.90
831	4.75	64.03	21.90	5.35	0.15	2.23	1.57	0.07	0.15	15.67	4783	15.1
834	4.76	61.21	20.89	8.44	0.52	2.28	1.57	0.29	0.16	18.60	6552	13.9
857	2.93	68.34	19.98	4.69	0.78	1.51	0.92	0.92	0.13	17.00	5292	9.63
881	4.13	60.85	22.16	8.28	0.48	2.28	1.43	0.42	0.13	25.97	5328	3.46

[a]X-ray fluorescence (courtesy, WVGES) and [b]atomic absorption spectrometry data.
** ND < 0.01.

Table 3
Variable loadings to the first eight PCs and their respective eigenvalues.

Variable	PC 1	PC 2	PC 3	PC 4	PC 5	PC 6	PC 7	PC 8
Quartz	−0.329	0.046	−0.031	−0.066	0.084	0.108	0.7	−0.078
K-Feldspar	−0.289	0.12	0.104	−0.165	−0.119	0.049	0.010	0.376
Plagioclase	−0.078	−0.443	−0.344	0.264	0.122	−0.218	−0.083	0.082
Illite	0.320	−0.051	−0.028	0.111	−0.10	0.181	0.053	0.170
Kaolinite	−0.001	0.218	0.376	0.500	−0.241	−0.549	0.037	0.033
Chlorite	0.265	−0.000	0.004	−0.308	0.228	−0.327	−0.403	−0.339
% K_2O	0.311	0.066	0.001	0.033	−0.060	0.187	−0.100	0.401
% SiO_2	−0.323	0.119	−0.123	−0.024	0.085	0.044	0.016	−0.175
% Al_2O_3	0.289	0.152	0.059	0.327	0.16	−0.117	0.156	0.087
% Fe_2O_3	0.241	−0.253	0.206	−0.233	−0.294	0.021	−0.167	0.234
% Na_2O	−0.091	−0.419	−0.376	0.222	0.121	−0.238	−0.080	0.225
% MgO	0.299	−0.176	0.079	−0.232	0.029	−0.112	−0.168	−0.106
% TiO_2	0.275	−0.050	0.125	0.053	0.352	0.010	0.497	−0.295
% CaO	−0.101	−0.363	0.085	0.015	−0.663	−0.026	0.124	−0.426
% P_2O_5	−0.037	−0.423	0.312	−0.261	0.163	−0.097	0.514	0.206
Total Se	0.17	0.270	−0.395	−0.197	−0.228	−0.271	0.202	−0.065
Total As	0.239	−0.071	−0.208	0.320	−0.114	0.502	0.054	−0.222
Se(IV)	0.157	0.167	−0.447	−0.252	−0.214	−0.206	0.375	0.16
Eigenvalue	8.6095	2.8593	1.8580	1.1147	0.9099	0.8283	0.4919	0.3583
Proportion	0.478	0.159	0.103	0.062	0.051	0.046	0.027	0.020
Cumulative	0.478	0.637	0.740	0.802	0.853	0.899	0.926	0.946

All the ND values were replaced with zero values prior to computing PCA.

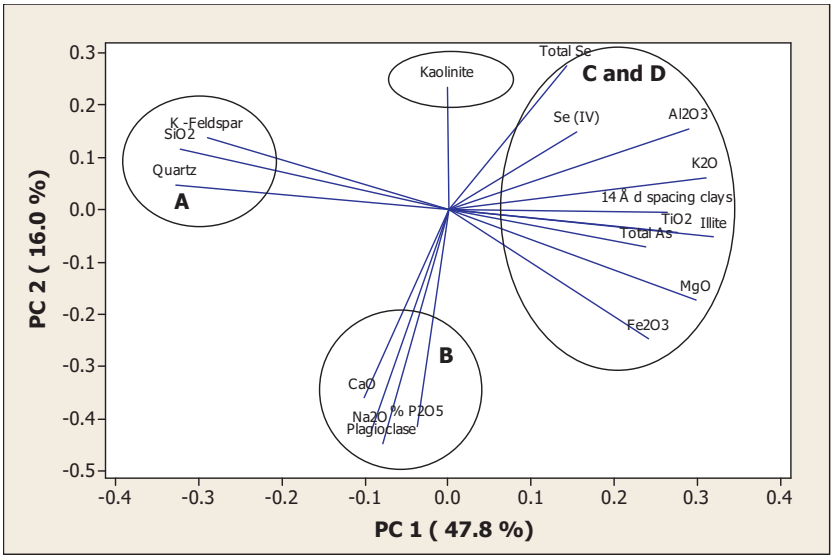

Fig. 1. Variable loading plot for PC 1 vs. PC 2. (A) Associated with K-Feldspar and quartz sandstones, (B) associated with plagioclase sandstones, (C) kaolinite and (D) associated with 14 Å *d*-spacing clays.

concentrations whereas the arsenic concentration clustered with the illite clay component. Kaolinite was negatively correlated with both arsenic and selenium concentrations as shown by the euclidean obtuse angles separating them. Therefore, kaolinite is not considered to be a critical clay component in rock minerals when considering selenium and arsenic pollution because no positive linear correlations were found between kaolinite with neither selenium nor arsenic (nor other elements as shown in Figs. 1 and 2). Such a two step application of PCA is a twofold process that initially groups similar parameters together in the first application followed by a further delineation of the grouped parameters in the second round to allow for a simplified interpretation of experimental data [16].

3.3. Scatter plots

Pearson correlations are applicable to normally distributed data where there is a linear relationship between variables [24]. The chemical data collected was initially standardized to ascertain normal distribution before the calculation of correlation coefficients.

3.3.1. Correlations for selenium

Although there is a non-linear global relationship between selenium and 14 Å *d*-spacing clays, it appears that the distribution of selenium in clays is dependent on rock lithology. The correlation coefficient between selenium and 14 Å *d*-spacing clays in claystones ($r = 0.84$, $p \leq 0.01$, $n = 7$) was the highest compared to shales ($r = 0.64$, $p \leq 0.05$, $n = 18$), sandstones ($r = 0.56$, $p \leq 0.01$, $n = 19$) and siltstones ($r = 0.76$, $p \leq 0.2$, $n = 4$). Negative correlation coefficients were obtained for selenium-plagioclase ($r = -0.1$, $p \leq 0.1$, $n = 47$) and selenium-K-Feldspar ($r = -0.33$, $p \leq 0.02$, $n = 47$). The correlation coefficients for selenium and kaolinite were: in claystones ($r = -0.56$, $p \leq 0.01$, $n = 7$), shales ($r = -0.2$, $p \leq 0.01$, $n = 18$), sandstones ($r = -0.58$, $p \leq 0.01$, $n = 19$) and siltstones ($r = -0.89$, $p \leq 0.2$, $n = 4$). Overall, there was a global negative correlation coefficient between selenium and kaolinite.

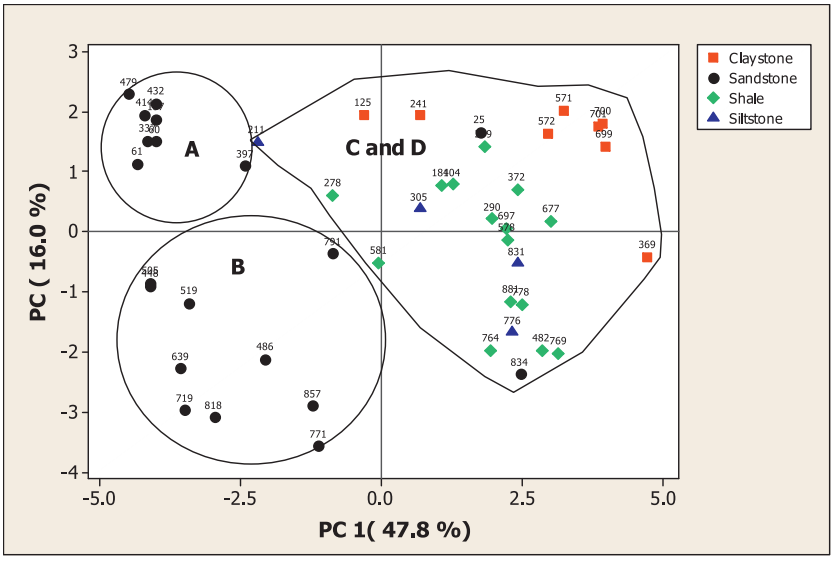

Fig. 2. A two dimensional sample score plot (total PC variance 63.7%). (A) associated with K-Feldspar and quartz sandstones, (B) associated with plagioclase sandstones, (C) kaolinite and (D) associated with 14 Å *d*-spacing clays.

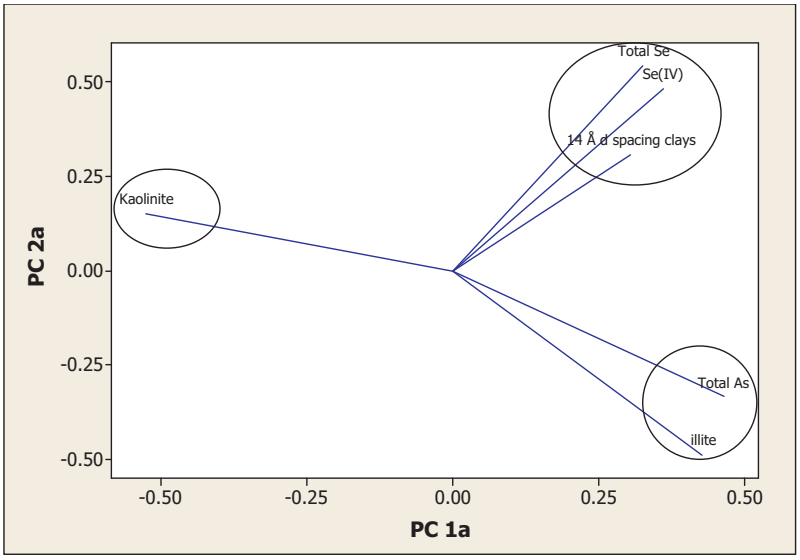

Fig. 3. Secondary PCA loading plot for major mineral inclusions with selenium and arsenic.

Total selenium concentrations had the following moderate correlations: K_2O ($r = 0.38$, $p \leq 0.009$, $n = 47$), Al_2O_3 ($r = 0.37$, $p \leq 0.01$, $n = 47$), MgO ($r = 0.2$, $p \leq 0.1$, $n = 47$), TiO_2 ($r = 0.19$, $p \leq 0.2$, $n = 47$), As (0.29, $p \leq 0.05$, $n = 47$) and Fe_2O_3 ($r = 0.067$, $p \leq 0.05$, $n = 47$). The close to zero correlation coefficient between Fe_2O_3 (or Fe) and total selenium indicate remote chances on the presence of ferrosellite ($FeSe_2$) as reported to be the major selenite constituent containing selenium in the US western phosphate rocks [25]. Other workers have also identified no correlation between sulfur and selenium to exist in the US eastern rocks [26] giving more evidence that selenium is not associated with Fe in pyrite or pyrrohotite in the rocks studied. The negative correlations between total selenium with kaolinite, quartz, K-Feldspar, and plagioclase could also indicate the absence of selenium in these rocks.

3.3.2. Correlations for arsenic

Positive correlations for arsenic with illite ($r = 0.80$, $p \leq 0.01$, $n = 47$) and with 14 Å *d*-spacing clays ($r = 0.31$, $p \leq 0.04$, $n = 47$) were observed.

Arsenic was found to have a higher positive correlation with plagioclase sandstones ($r = 0.79$, $p \leq 0.01$, $n = 11$) compared to non-plagioclase sandstones ($r = 0.52$, $p \leq 0.02$, $n = 37$). Arsenic concentrations had negative correlations with kaolinite ($r = -0.19$, $p \leq 0.2$, $n = 47$) and with K-Feldspar ($r = -0.70$, $p \leq 0.01$, $n = 47$). There were moderate correlations with MgO ($r = 0.50$, $p \leq 0.001$, $n = 47$), Fe_2O_3 ($r = 0.41$, $p \leq 0.001$, $n = 47$), Al_2O_3 ($r = 0.57$, $p \leq 0.001$, $n = 47$), K_2O ($r = 0.66$, $p \leq 0.001$, $n = 47$) and TiO_2 ($r = 0.53$, $p \leq 0.001$, $n = 47$).

3.4. Location of selenium and arsenic in the mineral lattice

3.4.1. Interlayer position

The presence of trace elements in minerals depends on the nature and the composition of clays. Illite and 14 Å *d*-spacing clays have been shown to contain most of the selenium and arsenic compared to kaolinite. Kaolinite was found to have negative correlations with selenium. As outlined in the previous section, positive correlations with selenium existed for 14 Å *d*-spacing clays and illite. It is therefore more likely that the presence of kaolinite reduces the abundance of the illite and 14 Å clays that do affect Se and As geochemistry, thus explaining the negative correlation with kaolinite. The presence of selenium and arsenic in illite and 14 Å *d*-spacing clays implies that there is a link between the microscopic structure of clays and elemental concentration. Kaolinite does not have an accessible interlayer but such an accessible interlayer is present in illite and the 14 Å *d*-spacing clays as shown in Fig. 4.

The presence of accessible interlayer in illite and 14 Å *d*-spacing clays is a clear distinguishing factor between the two classes of clays (1:1 and 2:1 types). This information points to the fact that arsenic and selenium could reside in the interlayer region of the illite and 14 Å *d*-spacing clays as previously suggested [2]. It has been reported that dissolved organic molecules [27,28] that may contain trace elements can sorb onto the clay minerals and subsequently enter the interlayer spacing where intercalation and lithification can occur.

3.4.2. Ionic substitution in the accessible interlayer

Ions with similar charge and are within 15% of their ionic radius can replace one another through isomorphous substitution/inclusion [6]. Thus resident ions in clays or any crystal lattice can be replaced by other ions of comparable size and charge without distorting the crystal lattice during the lithification stage. The ionic radii for K^+, Al^{3+} and Mg^{2+} and Ti^{4+} in crystal environments are 152, 67.5 and 0.745 pm, respectively [29]. The crystal radii for Fe^{2+} and Fe^{3+} are 0.75 and 0.69 pm for low spin and 0.92 and 0.79 pm in high spin environments [29], respectively. The crystal radii for selenium ions in are 184, 64 and 56 pm for Se(II), Se(IV) and Se(VI) in solid states respectively. Also, the crystal radii for As(III) and As(V) are 72 and 60 pm, respectively [29]. Therefore selenium ions could have been used in place of, or combined with Al^{3+} and Mg^{2+} during the formation of brucite and gibbsite in chlorite or in the uptake of Mg^{2+} in vermiculite because the ionic sizes of Al^{3+} and Mg^{2+} are close to those of Se(IV) and Se(VI). The selenium and arsenic ions could have also entered the interlayer regions independently.

3.4.3. Ionic substitution in the octahedral layers

The ions Al^{3+}, Mg^{2+}, Ti^{+}, Fe^{2+} and Fe^{3+} found in the clay octahedral layers have ionic sizes that are within 15% the sizes of As(III), As(V), Se(IV) and Se(VI). Both selenium and arsenic ions can also occupy the vacant dioctahedral positions or substitute ions within the octahedral positions. Ryan et al. [13] proposed that mineral sites identified as likely hosts for bicarbonate leachable arsenic included tetrahedral sites of antigorite or talc as As(V) substituted for Si(IV), octahedral sites of antigorite or talc as As(III) substituted for Mg(II), magnetite octahedral sites as As(III) substituted for Fe(III),

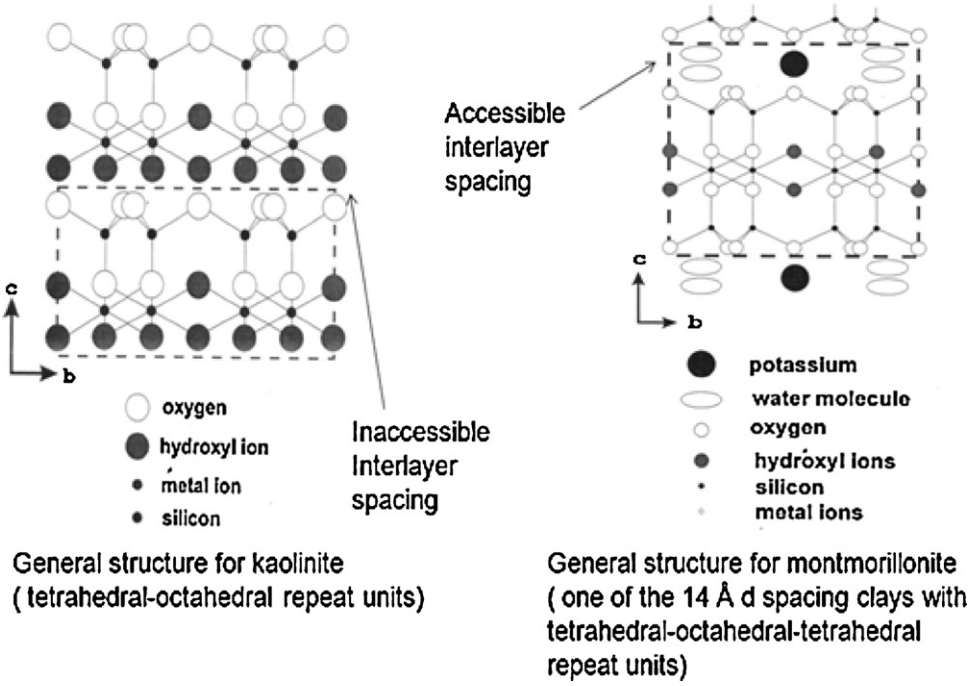

Fig. 4. General chemical structures of kaolinite and montmorillonite.

magnesite crystallographic sites, and adsorption onto mineral surfaces. Similar mechanisms may also occur for selenium species.

4. Priotization of waste disposal

Ziemkiewicz et al. [30] developed an in situ treatment of mining waste that immobilizes leached selenium on goethite (iron hydroxide) surfaces. A layer of goethite is deliberately placed first in a landfill before the introduction of selenium laden mining waste. The process resulted in 70% decrease in the concentration of dissolved selenium in the associated mine drainage. Both selenium and arsenic species can get sorbed through inner and outer sphere coordination onto the goethite chemical surface. Thus mining waste containing substantial amounts of illite and 14 Å *d*-spacing clays would have to be placed in landfills or valley fills containing more goethite because 14 Å *d*-spacing clays contain more selenium and illite has more arsenic. Using a combination of goethite and nanoparticles of titanium dioxide in the in situ treatment could result in a greater percentage of immobilized selenium. In laboratory environments, both rutile and anatase titanium dioxide nanoparticles have been used to sorb more than 90% of arsenic and selenium [31–33]. TiO_2 has high affinities for Se(IV), Se(VI), As(III), and As(V) that span from pH 3 to 9 [32,33]. Such a wide pH range covers the 6.5–8.5 pH values that are found in most natural aquatic environments. The binding of selenium and arsenic oxoanion species to TiO_2 nanoparticles has been shown to occur through inner sphere and outer sphere surface complexation via pH dependent surface hydroxyl groups [34].

5. Conclusion

A two step application of principal component analysis is a powerful technique that orthogonally decomposes data matrix to quickly identify clustering of samples and variables that are closely related allowing for enhanced chemometric analysis of experimental results. Although kaolinitic clays are major constituents of river sediments with substantially high adsorption capacities, they do not constitute the most important clay fractions that harbor highest leachable selenium and arsenic concentrations in MTR/VF sites. The same applies for quartz and K-Feldspars which correlated negatively with arsenic and selenium. On the other hand, plagioclase had a relatively high positive correlation with arsenic and this observation could be the reason why there were relatively high concentrations of arsenic in sandstones compared to selenium. The high positive correlation between illite and arsenic suggested that there are substantial amounts of arsenic that could be located in either the interlayer or the octahedral lattice of illite. The illite and 14 Å *d*-spacing clays are major constituents of claystones, shales, and siltstones. The information obtained indicates that the interlayer in 14 Å *d*-spacing and illite clays contains significant concentrations of selenium and arsenic, respectively. In general, "shales" (shales, claystones, and siltstones) were found to contain more leachable selenium compared to sandstones. The entry of these elements into the interlayer could have occurred during intercalation and lithification stages of sedimentary rock formation. We recommend the use a combination of both goethite and TiO_2 in the in situ treatment of mine wastes. We therefore propose that a greater proportion of leachable selenium species are contained within the silicate matrices of 14 Å *d*-spacing clays and that of leachable arsenic species are in illite.

Acknowledgements

We would like to thank the West Virginia Geological and Economic Survey for providing the pulverized rock samples and the United States Geological Survey – State Water Resources Research Institute Program for providing financial assistance for this research.

References

[1] G. Bryant, S. McPhilliamy, H. Childers, A Survey of the water Quality of Streams in the Primary Region of Mountaintop/Valley Fill Coal Mining, West Virginia Geological and Economic Survery (WVGES), 2002.
[2] M. Hardy, S. Cornu, Location of natural trace elements in silty soils using particle-size fractionation, Geoderma 133 (2006) 295.

[3] J. Satterberg, T.S. Arnarson, E.J. Lessard, R.G. Keil, Sorption of organic matter from four phytoplankton species to montmorillonite, chlorite and kaolinite in seawater, Mar. Chem. 81 (2003) 11–18.
[4] B.R. Simoneit, Molecular indicators (biomarkers) of past life, Anat. Rec. 268 (2002) 186–195.
[5] N. Noffke, G. Geddes, T. Klenke, Benthic cyanobacteria and their influence on the sedimentary dynamics of peritidal depositional systems (siliciclastic, evaporitic salty, and evaporitic carbonatic), Earth Sci. Rev. 62 (2003) 163–176.
[6] G. Faure, Principles and Applications of Inorganic Geochemistry, MacMillian Publishing Co., New York, 1991.
[7] A. Plancon, New modeling of X-ray diffraction by disordered lamellar structures, such as phyllosilicates, Am. Mineral. 87 (2002) 1672–1677.
[8] K.A. Eriksson, I.H. Campbell, J.M. Palin, C.M. Allen, B. Bock, Evidence for multiple recycling in neoproterozoic through Pennsylvanian sedimentary rocks of the central Appalachian basin, J. Geol. 112 (2004) 261–276.
[9] H. Park, D.L. Barbeau Jr., A. Rickenbaker, D. Bachmann-Krug, G. Gehreîs, Application of foreland basin detrital-zircon geochronology to the reconstruction of the southern and central Appalachian orogen, J. Geol. 118 (2010) 23–44.
[10] J.R. Price, M.A. Velbel, C. Patino, Rates and time scales of clay-mineral formation by weathering in saprolitic regoliths of the southern Appalachians from geochemical mass balance, Geol. Soc. Am. Bull. 117 (2005) 783–794.
[11] V. Peterson, J.G. Ryan, Petrogenesis and structure of the Buck Creek mafic-ultramafi csuite, southern Appalachians: constraints on ophiolite evolution and emplacement in collisional orogens, Geol. Soc. Am. Bull. 121 (2009) 615–629.
[12] C.S. Holm-Denoma1, R. Das, Bimodal volcanism as evidence for Paleozoic extensional accretionary tectonism in the southern Appalachians, Geol. Soc. Am. Bull. 122 (2010) 1220–1234.
[13] P.C. Ryan, J. Kim, A.J. Wall, J.C. Moen, L.G. Corenthal, D.R. Chow, C.M. Sullivan, K.S. Bright, Ultramafic-derived arsenic in a fractured bedrock aquifer, Appl. Geochem. 26 (2011) 444–457.
[14] M. Ringner, What is principal component analysis? Nat. Biotechnol. 26 (2008) 303–304.
[15] R. Faria, J.C. Duncan, R.G. Brereton, Dynamic mechanical analysis and chemometrics for polymer identification, Polym. Test. 26 (2007) 402–412.
[16] C.D. Adam, S.L. Sherratt, V.L. Zholobenko, Classification and individualisation of black ballpoint pen inks using principal component analysis of UV–vis absorption spectra, Forensic Sci. Int. 174 (2008) 16–25.
[17] K.R. Gabriel, The biplot graphic display of matrices with application to principal component analysis, Biometrika 58 (1971) 453–457.
[18] I. Pumure, J.J. Renton, R.B. Smart, Ultrasonic extraction of arsenic and selenium from rocks associated with mountaintop removal/valley fills coal mining: estimation of bioaccessible concentrations, Chemosphere 78 (2010) 1295–1300.
[19] ICDD, Powder Diffraction File, Alphabetical indexes, Inorganic phases, 1997.
[20] I. Pumure, J.J. Renton, R.B. Smart, Accelerated aqueous leaching of selenium and arsenic from coal associated rock samples with selenium speciation using ultrasound extraction, Environ. Geol. 56 (2009) 985–991.
[21] T. Ohta, H. Arai, Statistical empirical index of chemical weathering in igneous rocks: a new tool for evaluating the degree of weathering, Chem. Geol. 240 (2007) 280–297.
[22] C. Mosser, A. Brillanceau, Y. Besnus, Relationship between sediments and their igneous source rocks using clay mineral multi-element chemistry: the Cenozoic lacustrine Anloua basin (Adamaoua, Cameroon), Chem. Geol. 90 (1991) 319–342.
[23] J. Tessier, C. Duchesne, G. Bartolacci, A machine vision approach to on-line estimation of run-of-mine ore composition on conveyor belts, Miner. Eng. 20 (2007) 1129–1144.
[24] A.G. Asuero, A. Sayago, A.G. González, The correlation coefficient: an overview, Crit. Rev. Anal. Chem. 36 (2006) 41–59.
[25] A.L. Ryser, et al., Micro-spectroscopic investigation of selenium-bearing minerals from the Western US Phosphate Resource Area, Geochem. Trans. 6 (2005) 1–11.
[26] D.J. Vesper, M. Roy, C.J. Rhoads, Selenium distribution and mode of occurrence in the Kanawha Formation, southern West Virginia, U.S.A., Int. J. Coal Geol. 73 (2008) 237–249.
[27] M.J. Kennedy, D.R. Pevear, R.J. Hill, Mineral surface control of organic carbon in black shale, Science 295 (2002) 657–660.
[28] S.P. Indraratne, T.B. Goh, H. Shindo, Sorption of organic compounds by hydroxy-interlayered clays through chelation and humification processes, Geoderma 139 (2007) 314–320.
[29] R. Shannon, Revised effective ionic radii and systematic studies of interatomic distances in halides and chalcogenides, Acta Crystallog. A 32 (1976) 751–767.
[30] P.F. Ziemkiewicz, M. O'Neal, R.J. Lovett, Selenium leaching kinetics and in situ control, Mine Water Environ. 30 (2011) 141–150.
[31] M. Pena, X. Meng, G.P. Korfiatis, C. Jing, Adsorption mechanism of arsenic on nanocrystalline titanium dioxide, Environ. Sci. Technol. 40 (2006) 1257–1262.
[32] J.D. Peak, D.L. Sparks, Mechanisms of selenate adsorption on iron oxides and hydroxides, Environ. Sci. Technol. 36 (2002) 1460–1466.
[33] S. Li, N. Deng, Separation and preconcentration of Se(IV)/Se(VI) species by selective adsorption onto nanometer-sized titanium dioxide and determination by graphite furnace atomic absorption spectrometry, Anal. Bioanal. Chem. 374 (2002) 1341–1345.
[34] P.K. Dutta, A.K. Ray, V.K. Sharma, F.J. Millero, Adsorption of arsenate and arsenite on titanium dioxide suspensions, J. Colloid Interface Sci. 278 (2004) 270–275.